where

$$T_m=\boldsymbol{\Theta}_m\cdot\hat{e}_\perp,$$

$$S_m=\frac{1}{\zeta}(e^{-\zeta z_m}-e^{-\zeta z_{m+1}}),$$

$$C=e^2\omega\mu^2/(\pi^2\hbar c^3|\mu+\sigma|^2),$$

and the asterisk denotes complex conjugation.

The average of T_mT_n over the angular distributions may be shown to give $\frac{1}{2}(g_{mn})\langle\Theta^2\rangle_{\rm av}$, where $\langle\Theta^2\rangle_{\rm av}=\int d\Omega p(\Theta)\Theta^2$, and where $g_{mn}=\min(m,n)$. It was assumed in evaluating this average that the elastic scattering cross section is peaked strongly in the forward direction and hence that $\boldsymbol{\Theta}$ may be considered a two-dimensional vector perpendicular to $\hat{z}$.

The integrations over the z variables may be carried out explicitly and yield

$$J=\frac{C\langle\Theta^2\rangle_{\rm av}}{2|\zeta|^2}\sum_{m=1}^{\infty}\sum_{n=1}^{\infty}g_{mn}\times\{I_{mn}+I_{m+1,n+1}-I_{m+1,n}-I_{m,n+1}\},\quad\text{(A2)}$$

where

$$I_{mn}=\left(\frac{\gamma}{\gamma+2\,\mathrm{Re}\zeta}\right)^{g_{mn}}\times\left(\frac{\gamma}{\gamma+\mathrm{Re}\zeta+i\,\mathrm{sgn}(m-n)\,\mathrm{Im}(\zeta)}\right)^{|m-n|}.\quad\text{(A3)}$$

The function $\mathrm{sgn}(x)\equiv x/|x|$. The double sum may be evaluated without difficulty; the final result is

$$J=C\gamma\langle\Theta^2\rangle_{\rm av}/4|\zeta|^2\,\mathrm{Re}\zeta.\quad\text{(A4)}$$

It is clear that $\langle\Theta^2\rangle_l=\gamma\langle\Theta^2\rangle_{\rm av}$. Inserting the factor C into Eq. (A4), one finds Eq. (7). The averages over $d^2N_{\rm II}/d\omega d\Omega$ may be evaluated in the same manner as that sketched above.

PHYSICAL REVIEW VOLUME 135, NUMBER 3A 3 AUGUST 1964

Magneto-Optical Studies of the Band Structure of PbS

E. D. PALIK AND D. L. MITCHELL
U. S. Naval Research Laboratory, Washington, D. C.

AND

J. N. ZEMEL
U. S. Naval Ordnance Laboratory, White Oak, Silver Spring, Maryland

(Received 12 March 1964)

By a combination of interband and free-carrier experiments performed on epitaxial and bulk n- and p-type crystals, the energy-band parameters of PbS in the vicinity of the band edge have been determined at 77°K. Interband magneto-absorption measurements have established that the valence and conduction bands are nondegenerate (except for spin), approximately spherical and parabolic, and have extrema at essentially the same point in $\mathbf{k}$ space, probably the L points. Analysis of the data yields values for the energy gap, the reduced effective mass and also the effective g factors for both the valence and conduction bands. Measurements of the Burstein-Moss effect in the zero-field absorption edge indicate multiple bands, most likely at the <111> zone boundaries. The individual valence- and conduction-band effective masses were determined from free-carrier Faraday rotation measurements at a temperature slightly above 77°K. Additional structure in the rotation for p-type material indicates possible intervalence band transitions. The reversal of the interband Faraday rotation with carrier concentration and temperature is explained on the basis of the band structure determined here. The effects of strain and carrier concentration on the band parameters were also investigated and the effective deformation potential for dilation was determined.

I. INTRODUCTION

MAGNETO-OPTICAL experiments[1] provide a powerful tool for probing the band structure of semiconductors in the vicinity of band extrema. Cyclotron resonance[2] is particularly useful since it yields precise values for effective masses and their anisotropy. The free-carrier Faraday[3] and Voigt[4] effects, which arise from the dispersion associated with the cyclotron absorption lead to less detailed information, but are useful since they may be measured over a wider range of experimental conditions. The free-carrier experiments, however, suffer a limitation in that they only

[1] T. S. Moss, Phys. Stat. Sol. **2**, 601 (1962); B. Lax and S. Zwerdling, *Progress in Semiconductors* (John Wiley & Sons, Inc., New York, 1960), Vol. 5, p. 231.

[2] G. Dresselhaus, A. F. Kip, and C. Kittel, Phys. Rev. **98**, 368 (1955); E. Burstein, G. S. Picus, and H. A. Gebbie, *ibid.* **103**, 825 (1956).

[3] S. D. Smith, T. S. Moss, and K. W. Taylor, Phys. Chem. Solids **11**, 131 (1959).

[4] S. Teitler, E. D. Palik, and R. F. Wallis, Phys. Rev. **123**, 163 (1961); S. Teitler, Phys. Chem. Solids **24**, 1487 (1963).

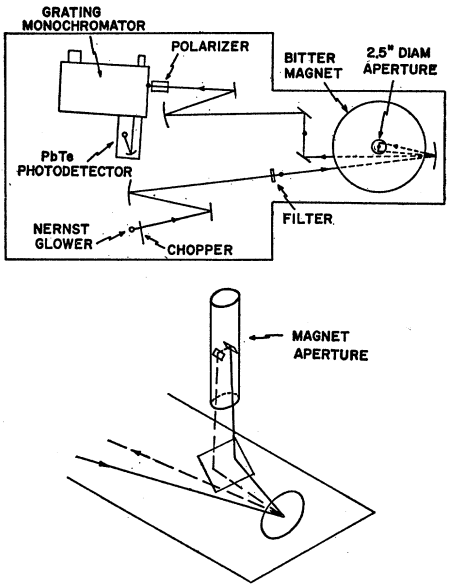

FIG. 1. A schematic diagram of the optical system used for the experiments in the NRL 2.5-in. Bitter-type magnet is shown in the upper figure. The lower figure indicates the light ray path in and out of the magnet.

probe the energy band in the vicinity of the Fermi energy. The addition of free carriers to raise the Fermi energy and probe further into the band may lead to misleading results, since the added charge centers can alter the energy states near the extremum[5] from those given by the empty lattice.

The interband magneto-optical absorption[6–8] and dispersion[9–11] experiments allow the bands to be probed over a wide range in energy with or without added free carriers in the bands. A precise value for the forbidden energy gap may be obtained and, for nondegenerate extrema, the effective g factors for valence and conduction band. The interband experiments also permit measurement of the reduced effective mass and its anisotropy. Since this mass is the reduced effective mass for both conduction electrons and holes, one of the effective masses must be found by some free-carrier experiment in order to calculate the other.

The masses, g factors, and energy gap are not unrelated. If the symmetry types and energy separations of all the energy bands at a particular point in $\mathbf{k}$ space are known, then it is possible to compute the band parameters by a suitable $\mathbf{k}\cdot\mathbf{p}$ perturbation calculation.[12] Conversely, given experimental values for the energy gap and for the g factors and effective masses of the valence and conduction bands, it is possible to limit the possible combinations of symmetry types and energy separations for the other interacting bands. Pikus and Bir[13] have calculated some of the mass parameters for various band models which apply to the NaCl-type lattice of PbS. However, their calculation does not include the effects of the other bands and does not specifically take into account the relativistic terms which Johnson, Conklin, and Pratt[14] have shown are important in the lead salts.

A combination of free-carrier magneto-optical, interband magneto-optical and zero-field optical experiments were chosen for this work in order to investigate the band structure of PbS at 77°K and determine the band parameters for the valence and conduction bands in the vicinity of their extrema.

The interband experiments were performed on both epitaxial crystals on NaCl substrates, which have recently become available,[15] and on a thicker natural crystal selected for its high-carrier concentration. The nature of the samples require subsidiary studies of the effects of strain and of high-carrier concentrations on the values for the band parameters.

The experimental procedures and results are presented in the sections on experimental methods, free-carrier magneto-optical experiments, zero-field absorption edge and interband magneto-optical experiments. The section on band structure summarizes the individual studies and discusses the band models which are consistent with the results. From the measurements it is possible to show that the valence- and conduction-band edges are nondegenerate (except for spin), are approximately parabolic and spherical at 77°K, and are located at essentially the same point in $\mathbf{k}$ space, most probably at the $\langle 111\rangle$ zone boundaries. Furthermore, the effective masses and also the effective g factors for the valence and conduction bands are approximately equal.

II. EXPERIMENTAL METHODS

A. Magneto-Optical Systems

The data were obtained using infrared optical system in conjunction with the Bitter-type, air-core, solenoidal magnets of the NRL magnet facility.[16] Most of the data were obtained with a "look through" magnet with a 2.5-in. cylindrical aperture. This magnet is capable of

[5] R. H. Parmenter, Phys. Rev. **104**, 22 (1956); P. A. Wolff, Phys. Rev. **126**, 405 (1962); E. O. Kane, in *Proceedings of the International Conference on the Physics of Semiconductors, Exeter, 1962* (The Institute of Physics and the Physical Society, London, 1962), p. 252.

[6] E. Burstein, G. S. Picus, R. F. Wallis, and F. Blatt, Phys. Rev. **113**, 15 (1959).

[7] L. M. Roth, B. Lax, and S. Zwerdling, Phys. Rev. **114**, 90 (1959).

[8] R. J. Elliott, T. P. McLean, and G. G. Macfarlane, Proc. Phys. Soc. (London) **72**, 553 (1958).

[9] I. M. Boswarva, R. E. Howard, and A. B. Lidiard, Proc. Roy. Soc. (London) **269**, 125 (1962).

[10] J. Kolodziejczak, B. Lax, and Y. Nishina, Phys. Rev. **128**, 2655 (1962).

[11] D. L. Mitchell and R. F. Wallis, Phys. Rev. **131**, 1965 (1963).

[12] E. O. Kane, Chem. Phys. Solids **1**, 82 (1956).

[13] G. E. Pikus and G. L. Bir, Fiz. Tverd. Tela **3**, 2090 (1962) [English transl.: Soviet Phys.—Solid State **4**, 1530 (1963)].

[14] L. E. Johnson, J. B. Conklin, and G. W. Pratt, Phys. Rev. Letters **11**, 538 (1963).

[15] R. B. Schoolar, J. D. Jensen, and J. N. Zemel, Bull. Am. Phys. Soc. **8**, 63 (1963).

[16] R. T. Swim, Rept. NRL Progr., November 1962, p. 1.

producing a steady field of 110 kOe at an expenditure of 3.0 MW of power. The remainder of the measurements were made either in a 4.25-in. magnet capable of 80 kOe or a 1.25-in. magnet capable of 150 kOe.

A typical 2.5-in. aperture optical system is shown in Fig. 1. The radiation from a Nernst glower source was chopped by a 13- or 310-cps chopper and was then directed by flat and spherical mirrors into the magnet from below. After passing through the sample in the transverse orientation, i.e., the direction of propagation perpendicular to the magnetic field, the radiation was directed out through the bottom of the magnet and finally to the entrance slit of a Perkin-Elmer grating monochromator equipped with a 150 lines/mm grating. The resolution attained was generally greater than 300.

The sample was mounted in a specially designed helium immersion Dewar which projected into the optical beam from above. Some of the measurements were performed with the monochromator in the fore optics. In some cases an Eastman Kodak filter transparent beyond 3 μ was placed in the beam before the sample in order to check for the presence of sample heating or higher orders of the grating. This was found to be unnecessary with the sample immersed directly in the coolant. With the sample mounted on a cold finger, heating effects were observed. In all cases, the sample itself effectively filtered the higher grating orders.

Linearly polarized radiation was obtained with a five-sheet AgCl pile-of-plates polarizer placed at the entrance slit of the monochromator. This polarizer together with a NaCl Fresnel rhomb was used to provide circularly polarized radiation in certain of the measurements performed with the sample in the longitudinal orientation in the 1.25-in. magnet.

The entire optical system was enclosed in a plexiglass "dry box." In those cases where water vapor was objectionable, the moisture was removed from the air by a commercial molecular sieve. It was also possible to eliminate much of the 4.2 μ CO_2 absorption from a 6-m path length by purging the air with gaseous N_2 driven off from liquid nitrogen containers within the box.

B. Electronic Systems

A Reeder thermocouple detector and standard 13-cps Perkin-Elmer electronics were used in the free-carrier experiments. This system was also used with a cooled PbTe detector for some of the interband experiments. The rest of the interband experiments were done with an improved system which utilizes the Princeton Applied Research Corporation lock-in amplifier as the major component. This system may be operated at higher frequencies in order to take advantage of the improved signal-to-noise ratios of photoconductive and photovoltaic detectors due to the $1/f$ noise characteristics of these detectors.

In operation, the output of a photoconductive PbTe or photovoltaic InSb detector was fed through a Tektronix No. 122 preamplifier into the PAR No. JB-5 lock-in amplifier. A PbS detector, placed in front of the 310-cps chopper, provided the reference signal for the lock-in amplifier. The output of the lock-in amplifier was fed into a Moseley No. 4-S recorder for presentation as a function of the magnetic field, or it was fed into a Brown recorder for presentation as a function of the wavelength. A Sanborn "fifo" amplifier isolated the x-y recorder from the current shunt used to measure the field.

C. Optical Dewars

The samples for the free-carrier experiments were mounted on a cold finger in a conventional optical double-Dewar. While this does not provide positive temperature control, it is adequate for these measurements due to the weak temperature dependence of the effective masses. From previous experience the sample temperature was estimated to be within 10°C of the temperature of the coolant.

For the interband experiments much better temperature control is required because of the sensitivity of the band-gap energy to small temperature changes. To insure constant and known temperatures for these experiments, the sample was immersed directly in the liquid nitrogen coolant in an optical double-Dewar specifically designed for this purpose. The Dewar was equipped with a removable inner end-cap fitted with two circular windows of sapphire or CaF_2 held in place with an epoxy cement.[17] This inner cap was connected directly to the cryogenic chamber with a gold "O" ring seal. Both seals, when fresh, readily withstood cooling to 4.2°K. The gold seal withstood repeated cycling between 300 and 4.2°K while the epoxy seals generally failed after the second or third cycle. Precautions must be taken to properly anneal the gold ring and provide a uniform thin rim of epoxy cement with no large blobs.

The sample, on a suitable holder, was inserted through the top of the Dewar through the liquid until it fitted into place in the optical beam. With allowance for sufficient clearance between the sample and cold windows, only fine bubbles were present. This bubbling introduced a tolerable amount of noise in the recorded spectra. With insufficient clearance, large bubbles appeared in the liquid nitrogen which regularly formed and passed through the optical beam causing periodic blips. Occasionally, the bubble would hover in the region of strongest magnetic field at the optical window. When the field was reduced, the bubble would rise. This behavior is due to the apparent paramagnetism of the gaseous "hole" when surrounded by a diamagnetic liquid.

D. Optical Samples

The thin PbS samples were ⟨100⟩ oriented, epitaxial crystals grown on rock-salt substrates by Schoolar,

[17] C. J. Ranch and W. C. Kernan, J. Appl. Phys. **33**, 496 (1962).

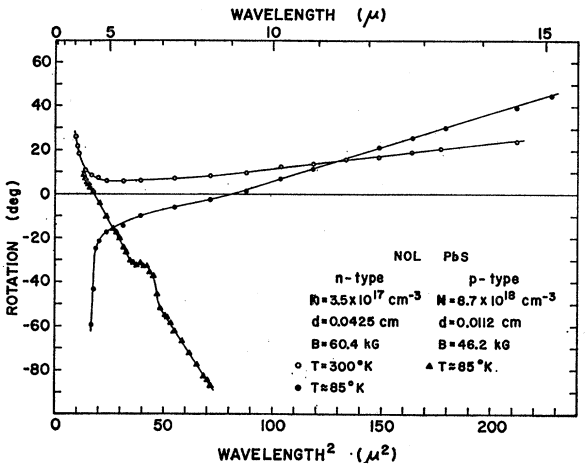

FIG. 2. Free-carrier Faraday rotation for n- and p-type PbS. Note the reversal in sign of the interband Faraday rotation at short wavelengths for the n-type sample at low temperatures. Also note the structure in the free-carrier rotation for the p-type sample.

Jensen, and Zemel[15] at the Naval Ordnance Laboratory. The films had electrical and optical properties similar to those of bulk single crystals. Laue photographs and Bragg diffractometer recordings indicate that the films are cubic, single crystals having the lattice constant of PbS, to within the experimental error of 0.1%. The films used ranged in thickness from 2 to 5 μ and exhibited interference fringes characteristic of an ideal optical thin film.[18] The films appeared to be strain free at room temperature and also gave reproducible results with repeated immersions into the cryogenic liquid. Eventually the films became mechanically damaged and began to peel from the backings.

The thicker PbS optical samples were prepared by conventional cleaving, grinding, and polishing techniques. These samples were either mounted on CaF_2 or NaCl backings with a thermoplastic cement, cellulose caprate, or in a few cases, freely mounted. The thickness of the samples was measured with a micrometer.

In the lead salts, excess carriers arise from impurities in the lattice as well as nonstoichiometry. To clarify our terminology, we will refer to crystals with low-carrier concentrations as being "purer" than higher carrier-concentration crystals. We realize that the reduction in carrier concentration might well be due to compensation of impurities. However, for conciseness we will make use of the above convention. The characteristics of the epitaxial, natural, and synthetic crystals from the Naval Ordnance Laboratory are listed in Table I together with the characteristics of the natural crystals obtained from the Smithsonian Institution.

TABLE I. Summary of properties of PbS samples.

Sample number	Type	Carrier concentration (10^{18} cm^{-3})	μ (300°K) (cm^2/V-sec)	μ (77°K) (cm^2/V-sec)
NOL-P	Grown p	8.7	550	
NOL-N	Nautral n	0.35	400	5670
SI-Wisconsin	Natural n	6.0	440	9570
NOL-108	Epitaxial p	0.35	505	4000
NOL-32	Epitaxial n	1.1	507	3710
NOL-30	Epitaxial n	1.5	450	3200
NOL-28	Epitaxial n	0.06		

[18] H. R. Riedl and R. B. Schoolar, Phys. Rev. **131**, 2082 (1963).

III. FREE-CARRIER MAGNETO-OPTICAL EXPERIMENT

A. Faraday Rotation

Since the interband experiments give values for reduced effective masses, it was necessary to measure some free-carrier magneto-optical effect to determine the conduction and/or valence-band effective mass, independently. When one is determined, the other may be calculated using the reduced effective mass.

Previous Faraday rotation experiments[19,20] have determined that the room-temperature effective mass for n-type samples in the carrier concentration range 1×10^{17}–2×10^{19} is $(0.17\pm0.01)m_0$. Near liquid-nitrogen temperature, the mass was observed to decrease to about $(0.12\pm0.01)m_0$. These measurements give an average of the mass over all directions of the wave vector $\mathbf{k}$ but do not determine the anisotropy or the position of the bands in $\mathbf{k}$ space. In view of the interband magneto-absorption data and zero-field absorption measurements discussed in the following sections, these values can be considered to be the effective mass for near spherical, parabolic conduction bands located along $\langle 111\rangle$ axes.

In addition to the results reported in Ref. 20, we have measured the Faraday rotation in samples of bulk n- and p-type PbS obtained from the Naval Ordnance Laboratory which contained 3.5×10^{17} and 8.7×10^{18} carriers/cm^3, respectively. Measurements were made with a Perkin-Elmer monochromator equipped with a NaCl prism and with polyethylene and AgCl pile-of-plates polarizers. The Bitter-type solenoidal magnet with a 4.25-in. cylindrical aperture was used. Results of these measurements for n-type PbS at room temperature and for both n- and p-type PbS near liquid-nitrogen temperature are shown in Fig. 2. The results for n-type PbS at room temperature are straightforward and show the strong positive interband rotation at short wavelengths and the positive free-carrier rotation at longer wavelengths. In a plot of θ versus λ^2, the free-carrier rotation may be extrapolated back to zero. The raw data of Fig. 2 must be corrected for the slight linear

[19] A. K. Walton, T. S. Moss, and B. Ellis, Proc. Phys. Soc. (London) **79**, 1065 (1962).

[20] E. D. Palik, S. Teitler, B. W. Henvis, and R. F. Wallis, in *Proceedings of the International Conference on the Physics of Semiconductors, Exeter 1962* (The Institute of Physics and the Physical Society, London, 1962), p. 288.

decrease in index of refraction as a function of λ^2. This variation has been measured by Riedl, Berk, and Dixon.[21] This correction allows $n\theta$ versus λ^2 to be plotted, the straight line portion of which yields an effective mass of $(0.177\pm0.01)m_0$.

Upon cooling this n-type PbS sample to low temperature, the interband rotation reverses sign. The reversal is discussed in Sec. V. The straight line portion does not extrapolate through zero, even when the index of refraction correction is made implying that there is a large interband rotation which persists to long wavelengths and decreases very slowly. The slope of a straight line through zero which asymptotically approaches the free-carrier rotation at longer wavelengths has been used to determine a low-temperature effective mass of $(0.118\pm0.01)m_0$.

At the moment we can only qualitatively account for the large decrease in mass with decreasing temperatures as due to the dependence of mass on the energy gap E_g. Subsequent work described in this paper seems to rule out significant nonparabolic effects or the emptying of carriers from one band into another as being responsible for the observed mass variation.

The room-temperature rotation in p-type PbS did not yield an effective mass because of the presence of a large superposed rotation, probably due to intervalence band transitions, in the region 5–8 μ. Similar structure has been observed by Walton and Moss[22] for the $V_3 \rightarrow V_1$, V_2 intervalence band transitions in p-type germanium. Upon cooling to low temperature, this added rotation was reduced greatly, and the typical free-carrier rotation was observed. The additional rotation may be seen in Fig. 2 superposed on the free-carrier rotation. As no index-of-refraction data were available, the index was assumed to be 4 and no correction for the variation in the index was made for the p-type data. The slope of a straight line through zero which asymptotically approached the free-carrier rotation yielded an effective mass of $(0.115\pm0.01)m_0$, essentially the same as the conduction mass. It is to be noted that the slopes of the straight line portions of the rotation in Fig. 2 differ only by a few percent from the "corrected" slopes used to obtain the effective mass. The estimate of uncertainty of $\pm0.01m_0$ comes primarily from uncertainty in the carrier concentration and in the slope. The interband rotation was always positive in the one p-type sample measured.

IV. ZERO-FIELD ABSORPTION EDGE

Optical measurements of the absorption edge of PbS have been made by Gibson[23] at room temperature and low temperatures, and by Scanlon[24] at room temperature. While these experiments have been useful in establishing the band gap at various temperatures, they did not reveal the important feature of the shift of the optical band edge with free-carrier concentration, the Burstein-Moss effect.[25,26] This effect has been studied in a number of the III–V compounds.[27–29] The results require a somewhat cumbersome analysis due to the complex valence band structure of these materials. The nondegenerate and parabolic band structure of PbS at 77°K, indicated by the magneto-optical data presented here, allows a more straightforward analysis.

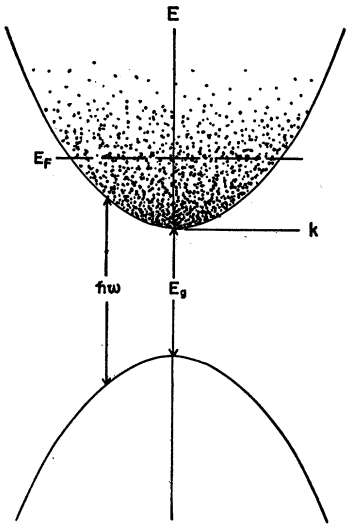

FIG. 3. E versus $\mathbf{k}$ diagram for simple valence and conduction bands with their extrema located at the same but arbitrary point in $\mathbf{k}$ space. The stippling in the upper band schematically represents the occupation of the available conduction-band states by the excess free carriers in the crystal. E_F labels the Fermi level in the conduction band, E_g the energy gap and $\hbar\omega$ the photon energy required for direct transitions to an arbitrary final state in the conduction band.

We have performed optical measurements of the band edge in both natural and epitaxial crystals of PbS. As shown by Palik,[30] and by Palik and Mitchell,[31] the absorption edge of PbS at liquid-nitrogen temperature is modified by the free carriers which fill available states in the conduction band. Analysis of this effect can lead to a determination of the number of equivalent bands involved in the transitions which give rise to the band-edge absorption.

We discuss the effect using a band model based on simple, spherical and parabolic conduction and valence bands located at the same point in $\mathbf{k}$ space, where $\mathbf{k}$ is the propagation vector. Such a band structure is shown schematically in Fig. 3. The strippled portion schematically represents the filling of some of the available states with free carriers. In pure material, the interband absorption constant for direct, allowed transitions is of the form

$$\alpha(\hbar\omega)=C(\hbar\omega-E_g)^{1/2}/\hbar\omega\,, \qquad (4.1)$$

[21] H. R. Riedl, N. F. Berk, and J. R. Dixon, Bull. Am. Phys. Soc. 8, 517 (1963).
[22] A. K. Walton and T. S. Moss, Proc. Phys. Soc. (London) 78, 1393 (1961).
[23] A. F. Gibson, Proc. Phys. Soc. (London) 65, 378 (1952).
[24] W. W. Scanlon, Phys. Chem. Solids 8, 423 (1959); Phys. Rev. 109, 47 (1958).
[25] E. Burstein, Phys. Rev. 93, 632 (1954).
[26] T. S. Moss, Proc. Phys. Soc. (London) 67, 775 (1954).
[27] W. Kaiser and H. Y. Fan, Phys. Rev. 98, 966 (1955).
[28] G. W. Gobeli and H. Y. Fan, Phys. Rev. 119, 613 (1960).
[29] J. R. Dixon and J. E. Ellis, Phys. Rev. 123, 1560 (1961).
[30] E. D. Palik, Naval Research Laboratory Progress Report, September 1963 (unpublished), p. 4.
[31] E. D. Palik and D. L. Mitchell, Conference on High Magnetic Fields, Oxford, 1963 (unpublished).

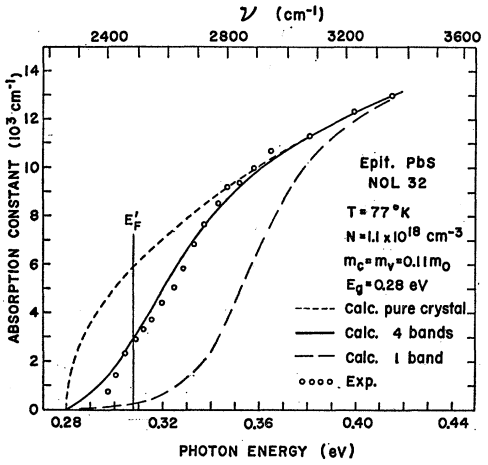

FIG. 4. The measured optical absorption edge in epitaxial PbS at 77°K showing the Burstein-Moss shift. Calculated curves for the absorption coefficient are shown assuming the free carriers to be in one parabolic and spherical band located at Γ or in four equivalent parabolic and spherical bands located at L.

where $\hbar\omega$ is the photon energy, E_g is the forbidden band gap, and C is a constant factor characteristic of the particular band structure. It involves the transition probability for the transition and the valence- and conduction-band density of states through the masses m_v and m_c. The presence of free carriers in the conduction band will modify this absorption. In PbS at these concentrations, the impurity band completely overlaps the conduction band. Because of the high static dielectric constant and the effective shielding of the excess charge centers by the free carriers, Coulomb shifts of the gap or modification of the underlying free-electron states[5] are not expected to be important for the range of concentrations discussed here. This is demonstrated experimentally in Sec. V where the energy gap determined magneto-optically at 77°K for a pure crystal is the same as determined for a crystal with 6×10^{18} carriers/cm³.

To lowest approximation, changes in the free-electron states and the transition probability between the states may be neglected. In this approximation, the absorption coefficient α_N may be written as the product of the absorption coefficient α_0 for the pure material times the Fermi distribution function for unoccupied states

$$\alpha_N(E)=\alpha_0(E)\{1+\exp[(E_F-E)/kT]\}^{-1}, \quad (4.2)$$

where $E_F=\hbar^2/2m_c(3N/8\pi M)^{2/3}$ is the Fermi energy for a total carrier concentration N distributed in M equivalent bands and E is the energy in the conduction band measured from the band edge. The conduction band energy E may be related to the photon energy $\hbar\omega$ for direct transitions if the energy spectrum of the bands is known. For parabolic energy bands, $(\hbar\omega-E_g)=(1+m_c/m_v)E$, so Eq. (4.2) may be rewritten:

$$\alpha_N(\hbar\omega)=\alpha_0(\hbar\omega)\left\{1+\exp\left[\frac{E_F'-(\hbar\omega-E_g)}{(1+m_c/m_v)kT}\right]\right\}^{-1}, \quad (4.3)$$

where $E_F'=[1+m_c/m_v]E_F$ is the photon energy relative to the band gap at which the absorption is just half the value for the pure crystal. This equation is given in a different form by Kaiser and Fan.[27] As given here, Eq. (4.3) preserves the form of Eq. (4.2), i.e., the product of the absorption for the pure crystal times the Fermi distribution function expressed in a transformed energy scale.

In the present experiments, the samples were immersed into liquid nitrogen to insure a definite, fixed temperature. The method of measurement was sample-in, sample-out. The reference path contained a piece of NaCl or CaF_2 equivalent to the backing on which the sample was mounted. Measurements were made in the spectral region 2–4.5 μ using a Perkin-Elmer monochromator equipped with a CaF_2 prism and a Reeder thermocouple. Corrections to the transmission due to the samples being mounted on backings of a different index of refraction and immersed into liquid nitrogen were not made since estimates indicated this to be negligible in the region of strong interband absorption. Also, no corrections have been made for free-carrier absorption, since calculations indicated that this absorption was also negligible compared to the interband absorption inside the band edge. It is, of course, not negligible outside the band edge. The thin films showed strong interference fringes at wavelengths longer than the band edge and even into the band edge until α became large enough to suppress multiple reflections inside the sample.

Results for an epitaxial film are shown in Fig. 4. The pure absorption edge was calculated with the band gap $E_g=0.28$ eV as determined from interband magneto-absorption measurements on the sample and with the assumption that the measured absorption constant at the highest photon energies was characteristic of the pure material. Then Eq. (4.1) was fitted through these end points. We have measured the absorption constant in another quite pure epitaxial film with $N=6\times10^{16}$ cm^{-3}, the results being in rough agreement with the calculated absorption constant for the pure material. The differences do not change the significant result of these measurements shown in Fig. 4. Taking the values $m_v=m_c=0.11m_0$ the modified band edge was calculated using Eq. (4.3) for $N=1.1\times10^{18}$ cm^{-3} and is shown by the dashed line assuming that one conduction band accounts for all the carriers. As can be seen, the fit is poor. However, assuming that the 1.1×10^{18} carriers/cm³ are distributed in four equivalent bands (implying ⟨111⟩ energy ellipsoids), the fit is much better. A somewhat less satisfactory fit to the data is obtained if three equivalent bands (implying ⟨100⟩ energy ellipsoids) are assumed although this possibility cannot be definitely excluded on the basis of this experiment alone. The values of α in the low-absorption-constant region (<2000 cm^{-1}) may be affected by the presence of interference fringes. Similar measurements were made on a natural sample with 6×10^{18} carriers/cm³ but only to

absorption constants as high as 500 cm^{-1}. These limited measurements also indicated multiple conduction bands.

It is interesting to note that at room temperature the edge absorption should be only slightly modified because the Fermi distribution function is smeared out. This may explain why previous work on band-edge absorption at room temperature has not revealed the Burstein-Moss effect clearly. Unless the absorption is measured fairly deep into the absorption edge to absorption constants much larger than a few hundred cm^{-1} and on several samples of different carrier concentration, this feature may be missed. Determination of the position of the band edge as a function of temperature from measurement of absorption constant in zero magnetic field may be difficult with PbS because as the sample cools, the edge shifts to lower photon energy but the Fermi distribution because sharper which tends to compensate for the gap shift.

The zero-field optical measurements indicate multiple conduction bands for PbS. Other evidence for ⟨111⟩ conduction-band minima has been obtained by Stiles, Burstein, and Langenberg[32] from de Haas–van Alphen susceptibility experiments and by Allgaier, Houston, Burke, Babiskin, and Siebenmann[33] from Schubnikov-de Haas magnetoresistance experiments.

The present optical measurements indicate that the large number of free carriers in the conduction band will affect the intensities of the interband magneto-absorption lines, as indeed does happen as will be discussed in Sec. V.

V. INTERBAND MAGNETO-OPTICAL EXPERIMENTS

A. Energy Levels in Magnetic Field

In the presence of an external magnetic field, the continuum of states in the valence and conduction band of a semiconductor are quantized into a set of semi-discrete Landau levels.[6] Near the extrema of energy bands these states may be characterized as one-electron states which retain their free-particle characteristics in the direction of the magnetic field and are quantized in cyclotron orbits in the plane perpendicular to the magnetic field. The Landau levels, labeled with the indices l and l' are shown in Fig. 5 for simple, parabolic valence, and conduction bands located at a symmetry point in $\mathbf{k}$ space such as Γ, L, or X. Symmetry requires that the bands have relative extrema at these points. As drawn here, the bands have their absolute extrema at the same point in $\mathbf{k}$ space, so that the minimum energy gap occurs for direct transitions.

In PbS, the energy gap most likely occurs at the ⟨111⟩ zone boundaries as discussed in Sec. IV. At these points in the Brillouin zone the bands have symmetries $L_6^{\pm}$ or

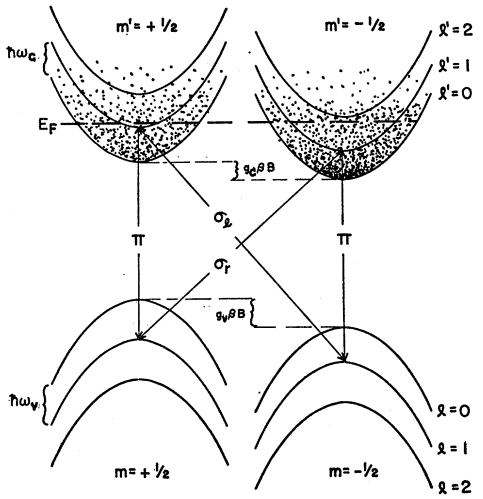

FIG. 5. E versus k_z diagram for simple and parabolic bands in the presence of a large magnetic field in the z direction. The spacing between adjacent Landau levels labeled by l or l' is the cyclotron energy $\hbar\omega_v$ or $\hbar\omega_c$. The gyromagnetic splitting of the individual Landau levels, labeled by the quantum numbers $m=\pm\frac{1}{2}$ or $m'=\pm\frac{1}{2}$, is given by $g_v\beta B$ or $g_c\beta B$ with the effective g factors both taken to be positive by the convention of Eq. (5.1). The sign of g_v as determined experimentally in PbS is negative. The stippling represents the occupation of the conduction band states by free carriers with a Fermi level E_F.

$L_4^{\pm}$, $L_5^{\pm}$ [13,14] and are nondegenerate except for the two-fold degeneracy resulting from time-reversal symmetry. In the presence of an external magnetic field the time-reversal degeneracy is lifted and the levels separate by an energy $g\beta B$ where g is the effective g factor, β is the Bohr magneton times Planck's constant, and B is the magnetic induction. This is shown in Fig. 5 as the double set of levels labeled with the indices m and m'.

The level scheme as drawn represents an ideal solid, i.e., a perfectly periodic potential and an infinite relaxation time. In a real crystal spatial inhomogeneities and the finite relaxation time will limit the definition of these states. The inhomogeneity broadening may be reduced by choosing suitable samples. The relaxation broadening, at a given temperature, generally cannot be reduced, so that it is necessary to apply magnetic fields large enough to satisfy the condition $\omega_i\tau_i\gg1$ where ω_i is the cyclotron frequency and τ_i is the relaxation time for the ith band. Since only a single valence or conduction band is considered here, the labels v or c are used for the band index. For interband transitions a similar condition may be specified $\omega_{vc}\tau_{vc}\gg1$, where $\omega_{vc}=\omega_v+\omega_c$ and $\tau_{vc}=\tau_v\tau_c/(\tau_v+\tau_c)$.

The Landau levels do not represent all of the final states available for excitation in the crystal. There exist localized states near impurities and imperfections and also exciton states[34] arising from the Coulomb attraction between a locally excited hole-electron pair.

[32] P. J. Stiles, E. Burstein, and D. N. Langenberg, J. Appl. Phys. Suppl. **32**, 2174 (1961).

[33] R. S. Allgaier, B. B. Houston, J. R. Burke, J. Babiskin, and P. G. Siebenmann, Bull. Am. Phys. Soc. **8**, 517 (1963).

[34] R. J. Elliott and R. Loudon, Phys. Chem. Solids **15**, 196 (1960).

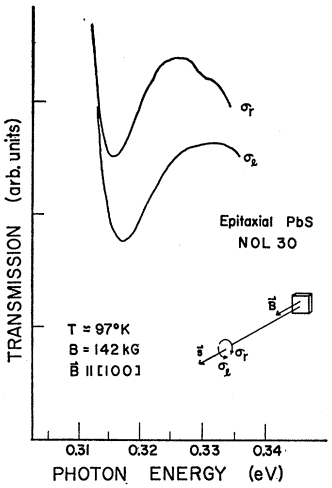

FIG. 6. Relative transmission for lcp and rcp radiation for the lowest, $l=0$ to $l'=0$, Landau transition. The scale is the same for both traces.

In addition, there exist many-electron "plasma" modes[35] which may be excited by proper polarization of the incident radiation. These effects are small in PbS and will be discussed later.

B. Selection Rules for Interband Transitions

The selection rules for interband transitions between Landau levels have been developed by several authors.[6–8] The selection rules for direct allowed transitions are $l'-l=0$ and $m'-m=0, \pm 1$, where l and l' represent the quantum number for a given Landau level and m and m' represent the quantized z components of the total angular momentum in the tight-binding limit. The selection rule $\Delta m=0$ applies for radiation propagating perpendicular to the direction of the magnetic field with the plane of polarization parallel to the magnetic field (π spectrum). The selection rule $\Delta m=\pm 1$ applies for radiation propagating in the direction of the magnetic field with left- or right-circular (lcp or rcp) polarization, respectively (σ_l and σ_r spectra). The electric vector of lcp radiation is defined as having the spatial profile of a left-hand screw. The σ spectrum, which is the superposition of the σ_l and σ_r spectra, is obtained with radiation linearly polarized perpendicular to the magnetic field and propagating perpendicular to the field.

This simple discussion applies to crystal wave functions that have the same symmetry properties as atomic wave functions characterized by an orbital quantum number l and a spin quantum number m. Both of the nondegenerate valence band states L_4^+ and L_5^+ given in Ref. 14 are linear combinations of spin-up and spin-down functions, so that the selection rules for transitions involving these states may be more complicated. If the simple selection rules are relaxed then four lines should be observed in both the σ and π spectra for transitions between a given pair of Landau levels. Only two lines were observed for each of the two orientations in PbS, so that it is assumed that the simple selection rules apply.

C. Coincidence of the Valence- and Conduction-Band Edges

The optical absorption arising from transitions between a given pair of Landau levels depends on the nature of the transition: whether it is direct or indirect, allowed or forbidden. Expressions for the direct and indirect transitions have been developed by Burstein, Picus, Wallis, and Blatt,[6] Elliott, McLean, and MacFarlane,[8] and Roth, Lax, and Zwerdling.[7] For indirect transitions the absorption increases by steps at the transition energies. This behavior has been observed at the indirect edge in germanium.[7] The predicted line shape for direct and allowed transitions shows a sharp peak at the minimum energy for transitions and an asymmetric tail to higher energies. The peak is due to the infinite (ideal case) density of states at the extremum of each Landau level. The asymmetric tail is due to direct transitions for initial states with k_z different from the extremal value. In the case of direct but forbidden transitions the character of the optical absorption depends on the polarization of the radiation: peaks for one direction of linear polarization and steps for the other.

Well-defined peaks in absorption were observed in PbS for all polarizations which indicated direct and allowed transitions between Landau levels. The lowest σ_l and σ_r lines, measured in transmission, are shown in Fig. 6. The absolute transmission was not measured, so that it is not possible to make a quantitative comparison of theoretical and experimental line shapes. Qualitatively, however, the observed shape agrees with the theoretical curves presented in Ref. 6 for approximately the same $\omega_{vc}\tau_{vc}$ condition. Other evidence that the transitions are direct-allowed has been given by Scanlon[24] and by Hall and Racette.[36]

The difference in strength for the σ_l and σ_r lines may be ascribed to the partial occupation of the conduction band states by free carriers. The stippling in Fig. 5 schematically represents the distribution of the free carriers over the states in the conduction band. If the gyromagnetic splitting of a given Landau level is appreciable compared to kT and if the level itself is within a few kT of the Fermi energy E_F, then the occupation of the two states will be significantly different. This difference is reflected in the absorption coefficient which is directly proportional to the density of unoccupied states in the conduction band.

[35] E. Burstein, P. J. Stiles, D. N. Langenberg, and R. F. Wallis, in *Proceedings of the International Conference on the Physics of Semiconductors, Exeter 1962* (The Institute of Physics and the Physical Society, London, 1962), p. 345.

[36] R. N. Hall and J. H. Racette, J. Appl. Phys. Suppl. **32**, 2078 (1961).

D. Nondegenerate Band Edges

The σ transmission spectra measured for a sample with a carrier concentration $N=1.1\times10^{18}$ cm^{-3} is shown in Fig. 7. The transmission has been normalized to the transmission at zero field. Well-developed transmission minima are observed. The lack of splitting in the σ spectra is due to the near coincidence of the σ_l and σ_r transitions as shown in Fig. 6. It may be observed that the spacing of the σ lines are uniform down to the lowest line which is partially obscured by the 4.2μ CO_2 absorption. The positions of the lines are given by the relation $\hbar\omega=E_g+(l+\frac{1}{2})\hbar\omega_{vc}$ where $\hbar\omega_{vc}=20$ meV. This simple behavior is only expected for parabolic and nondegenerate bands. For nonparabolic bands the cyclotron spacing varies inversely with the reduced effective mass. For degenerate bands the spacing of the lowest levels is nonuniform[6] and additional lines should appear as observed in germanium.[6] The lack of other than spin degeneracy is not surprising for energy band extrema located at the $\langle111\rangle$ zone boundary, since at this point the energy bands have symmetries[13,14] $L_6^{\pm}$ or $L_4^{\pm}$, $L_5^{\pm}$.

The lack of splitting of the σ spectra also indicates that the band edges either lie at $\mathbf{k}=0$ or along the $\langle111\rangle$ crystal directions. Bands lying in other crystal directions would be shifted unequally in energy by the large strain known to be present in these films.

E. Effective g Factors

In the presence of a magnetic field, the energy separation between a given pair of simple valence and conduction Landau states is given by the expression[6]

$$E_{ll'}=E_g+(l+\tfrac{1}{2})\hbar\omega_v+(l'+\tfrac{1}{2})\hbar\omega_c - g_v\beta Bm+g_c\beta Bm', \quad (5.1)$$

where l, l' quantum numbers label the given Landau subband in the valence and conduction band, respectively, g_v and g_c are the effective g factors for hole and electron, and β is the Bohr magneton times Planck's constant and B the magnetic induction. The quantum

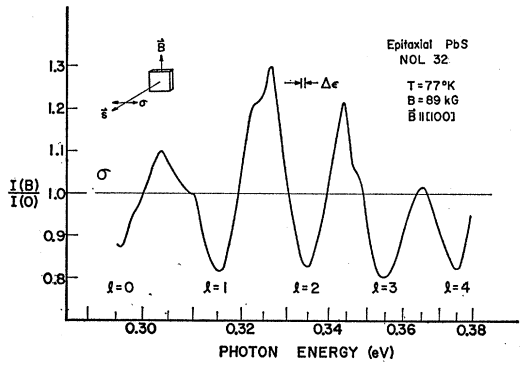

FIG. 7. The first five Landau transition lines are shown for a sample with $N>10^{18}$ cm^{-3}. The ratio of the transmission in magnetic field to the transmission in zero field is plotted at a fixed magnetic field. Note the even spacing and the absence of splitting for the σ lines.

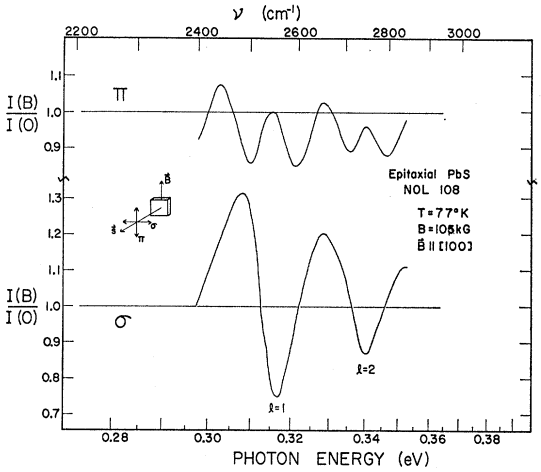

FIG. 8. The gyromagnetic splitting of the σ and π lines is shown for a sample with $N=3\times10^{17}$ cm^{-3}.

numbers m and m' refer to the z components of the total angular momentum operator and, for simple bands, take on values $\pm\frac{1}{2}$. The sign convention we have chosen for the valence band g factor in Eq. (5.1) follows Ref. 6.

The selection rules for the σ spectrum require that $\Delta l=0$ and $\Delta m=\pm1$ for lcp and rcp radiation, respectively. For a given l, the two transitions differ in energy by $(g_v+g_c)\beta B$. Similarly, the selection rules for the π spectrum lead to two transitions that differ in energy by $(g_v-g_c)\beta B$. The lack of splitting in the σ spectrum shown in Fig. 8 indicates that the g factors for the hole and electron are approximately equal and opposite in sign. This is verified by the separate measurement of the σ_l and σ_r spectra which are presented in Fig. 6. The measured value for the π splitting, shown in Fig. 8 may be combined with the measured value of the σ splitting to give the magnitudes of the hole and electron g factors.

The signs of the g factors may be obtained by further analysis of Fig. 6 by taking into account the effects of the free carriers in the conduction band. If the g factor for the conduction band is positive as shown in Fig. 5 then the final states for the σ_r transitions will lie to lower energy than the final states for the σ_l transitions. The free carriers will selectively populate the lowest level and consequently partially block optical transitions to these states. The population difference may become quite appreciable. At 100 kOe the level splitting of the conduction band is approximately equal to kT, so that the σ_r transition should be appreciably weaker than the corresponding σ_l transition. This is observed experimentally as shown in Fig. 6 indicating that the g factor for the conduction band is positive. The g factor for the valence band, therefore, is negative according to the convention we have chosen. The values for the g factors are given in Table II. These values are somewhat larger than those reported earlier[37] due to the improvement

[37] D. L. Mitchell, E. D. Palik, J. D. Jensen, R. B. Schoolar, and J. N. Zemel, Phys. Letters 4, 262 (1963).

TABLE II. Band parameters of PbS at 77°K.

Sample number	E_g (10^{-3} eV)	$Z_{vc}{}^p$ (eV)	m_{vc} [100]^a ($10^{-3}\,m_0$)	m_{vc} [110]^a ($10^{-3}\,m_0$)	g_v	g_c
SI-Wisconsin	309±5	4.3±0.6	54.5	50.8	−8.5±1.5	10.0±1.5
NOL-108 (Free)	307±3		55.2			
NOL-108 (Epit.)	278±2		51.5			
NOL-32 (Epit.)	280±2		49.3		−3.8[b]	5.3[b]
NOL-30 (Epit.)	278±2		51.0			
NOL-P	$m_v{}^F=(0.115\pm0.01)m_0$[c]					
NOL-N	$m_c{}^F=(0.118\pm0.01)m_0$[c]					

[a] Calculated from the average line spacing at 100 kG with the magnetic field directed along the indicated crystal direction.
[b] Line splitting not fully resolved.
[c] At temperature slightly above 77°K.

in the $\omega_{vc}\tau_{vc}$ condition for the π lines which was attained with later samples.

F. Energy Gaps

A plot of the energies of the absorption maxima as a function of the magnetic field is shown in Fig. 9 for the same sample as shown in Fig. 8. The lines exhibit the expected linear dependence on magnetic field and all extrapolate to a value $E_0=(0.278\pm0.002)$ eV. The exciton binding energy in PbS calculated using the measured reduced effective mass and the static dielectric constant is less than 10^{-4} eV. Although the binding energy increases with magnetic field, the magnitude remains negligible compared to the width of the lines themselves. The energy E_0, therefore, should represent the energy gap at 77°K for the epitaxial crystal on a NaCl substrate.

To investigate the effect of the strain on the energy gap and to verify that the lines themselves were not being split by strain in the epitaxial crystals, measurements were performed on an epitaxial film freed from its backing and on a natural crystal of cleaved PbS which was 150 μ thick. The interband absorption in this natural crystal was reduced by the presence of 6×10^{18} free-carriers/cm^{-3} in the conduction band, which permitted transmission measurements over a range of photon energies above the energy gap[30] as described in Sec. IV. A representative trace of the transmission at fixed photon energy is shown in Fig. 10 as a function of the magnetic field. Well-developed absorption maxima are observed which indicates that the relaxation time is not seriously affected by the additional charge centers and free carriers at these concentrations. The positions of the absorption maxima, or transmission minima, are plotted in Fig. 11. The line positions have been corrected for the variation of $\omega_{vc}\tau_{vc}$ across the width of the line by a procedure discussed in Sec. VG. This correction affects the effective-mass determination but does not alter the value obtained for the energy gap

$$E_g=(0.309\pm0.005)\text{ eV}.$$

The similarity of this curve to Fig. 9 indicates that the same transitions are being observed in both cases, i.e., the strain in the epitaxial layers does not shift bands unequally and introduce additional lines. The difference between the values for the energy gap is due to impurity and/or strain effects. The strain in the

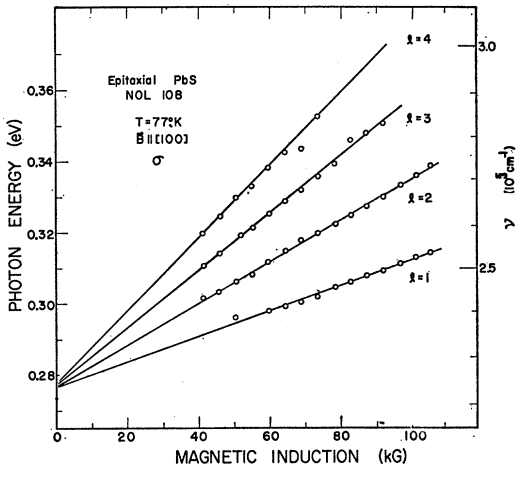

FIG. 9. The position in energy of the Landau transitions are plotted as a function of the magnetic induction for a low-carrier concentration epitaxial crystal. The value for the energy gap, obtained from extrapolation of the line to zero field, and the value for the reduced effective mass, obtained from the line spacing, are characteristic of the strained crystal.

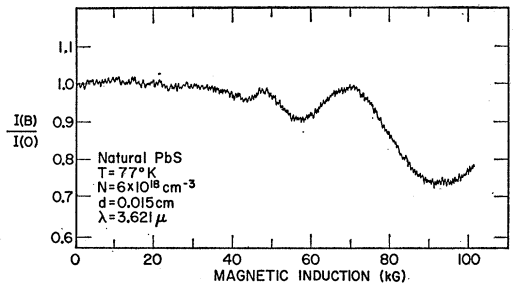

FIG. 10. A trace of the ratio of transmission as a function of the magnetic induction at a fixed photon energy for a thick natural crystal with $N=6\times10^{18}$ cm^{-3} carriers. The position of the Landau transitions is taken to be the points of tangency of this trace with the envelope curve as described in the text.

natural crystal should be negligible due to its thickness. The impurities, however, may alter the energy gap from that of a pure material by the Coulomb interaction with the fixed-charge centers and associated free carriers as discussed in Ref. 5. These effects are not considered to be important in PbS at these carrier concentrations due to the effective screening of the Coulomb field of the impurities by the large dielectric constant.

1. *Impurity Effects*

The effect of impurities on the energy gap has been studied by comparing the values obtained for two classes of crystals; strained crystals (as-grown epitaxial crystals) and unstrained crystals (free epitaxial and thick natural crystals). The observed energy gaps are given in Table II. Within each class, the values agree within experimental error. The same agreement is also obtained on a given sample for different runs. This indicates that the temperature and strain produced by direct immersion of the sample in the coolant are both reproducible. The results also indicate that the impurities have negligible effect on the band gap for concentrations up to 6×10^{18} cm^{-3}. The value $E_g=(0.307\pm0.003)$ eV obtained for the free epitaxial film, therefore, should be the energy gap for pure and unstrained PbS at 77°K. The difference between this value and the values obtained for the epitaxial crystals on substrates may be attributed entirely to the strain present in these crystals.

2. *Strain Effects*

The difference in the measured energy gaps is fairly substantial as can be seen by comparing the values given in Table II, the difference being about 29 meV. The most obvious source of so large a band gap difference is the thermally induced strain in the film. Oriented overgrowths of the epitaxial film type are generally bound tenaciously to the substrate. If the substrate and the film have different thermal expansion coefficients, they will generate strains in each other. If the film is sufficiently thin so that the traction which the stretched PbS film applies to the face of the NaCl substrate does not significantly deform the NaCl crystal, then the strain components in the plane of the film are given by

$$\epsilon_1=\epsilon_2=\int_{T_1}^{T_2}[\alpha_G(T)-\alpha_S(T)]dT, \qquad (5.2)$$

where α_G and α_S are the linear thermal expansion coefficients for PbS and NaCl, respectively, and T is the temperature. Also, if the film is sufficiently thin, then the strain components will be uniform across the thickness of the film and it may be treated as a uniform plate stressed by the lateral stress components $Q_1=Q_2=Q$. The films used in these experiments were of the order of microns in thickness while the lateral dimensions of the films and the thickness of the substrates were of the order of millimeters so that the thin-film approximations should hold. Solutions for the strains in thicker plates with traction applied to one face have been developed by Dougall[38] for isotropic and elastic media.

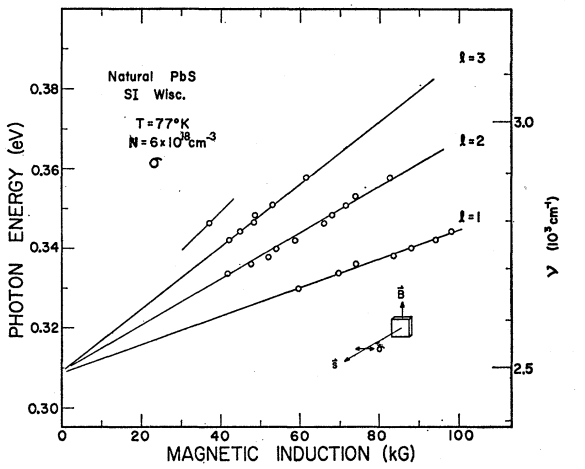

FIG. 11. The transition energies are plotted as a function of the magnetic induction for the same sample as in Fig. 10. The extrapolated energy gap and reduced effective mass, determined from the line spacing, have values characteristic of an unstrained crystal.

The other strain components in the film may be determined, under the thin-film assumption, by using the stress-strain relation[39]

$$\epsilon_i=s_{ij}Q_j, \qquad (5.3)$$

where ϵ_i are the strain components, Q_j are the stress components and s_{ij} are the compliance constants defined in the usual manner.[39] Once the strain components are known, the gap shift δE may be calculated by the equation

$$\delta E=\sum_{i=1}^{6}\epsilon_i Z_i, \qquad (5.4)$$

where the Z_i are deformation potentials defined by Herring and Vogt[40] for individual bands but here taken to represent the combined effective deformation potentials for interband transitions.

The epitaxial crystals used in these experiments were all oriented with the (001) plane keyed to the (001) plane of the NaCl so that the strain components $\epsilon_1=\epsilon_2=(s_{11}+s_{12})Q$ and $\epsilon_3=2s_{12}Q$ with the other components equal to zero. For $\langle111\rangle$ energy ellipsoids,[40] the deformation potentials $Z_1=Z_2=Z_3=Z^p$ so that the gap shift may be written $\delta E=2(s_{11}+2s_{12})QZ^p$. The deformation potential which appears for this particular two-dimensional dilation is the same that appears in the

[38] J. Dougall, Edin. Roy. Soc. Trans. **41**, 129 (1903).

[39] H. B. Huntington, in *Solid State Physics*, edited by F. Seitz and D. Turnbull (Academic Press Inc., New York, 1958), Vol. 7, p. 214.

[40] C. Herring and E. Vogt, Phys. Rev. **101**, 944 (1956).

expression for the gap shift from pressure experiments $\delta E=3(s_{11}+2s_{12})QZ^p$. This is not the case for ⟨100⟩ energy ellipsoids or for ⟨111⟩ ellipsoids for strains with other than ⟨100⟩ symmetry.[40]

We have calculated the effective deformation potential Z^p using the experimentally measured gap shift of (29±3) meV. The thermally induced strains were determined by numerically integrating Eq. (5.2) using the experimentally measured thermal expansion coefficients for[41] PbS and NaCl.[42] The value $\epsilon_1=\epsilon_2=(3.22\pm1.5)\times10^{-3}$ was obtained at 77°K. The high-temperature limit on the integral in Eq. (5.2) was taken to be 300°K based on the data of Reidl and Schoolar.[18] They observed that the peak in the index of refraction associated with the energy gap occurred at the same energies for both epitaxial films and bulk crystals. If there was a residual thermally induced strain at 300°K, the peak in the film could have been displaced to lower energies. Using the above values, the effective deformation potential $Z^p=4.3$ eV was calculated at 77°K with the cumulative error estimated to be 15%. This may be compared with the value $Z^p=3.45$ eV calculated from the value of $(\partial E_g/dP)_T=-8\times10^{-6}$ eV-cm²/kG measured by Paul, DeMeiss, and Finegold[43] at room temperature. The values for the compliance constants of PbS used in these calculations,

$$s_{11}=(7.1\pm0.1)\times10^{-13}\ \text{cm}^2/\text{dyne}$$

and

$$s_{12}=(0.4\pm0.6)\times10^{-13}\ \text{cm}^2/\text{dyne}$$

were calculated from the ultrasonic wave velocity measurements recently published by Chudinov.[44]

The method of measuring deformation potentials used here is direct and also potentially very accurate. The transverse strain components ϵ_1 and ϵ_2 may be determined directly with an accuracy limited only by the accuracy of the measured values for the thermal expansion coefficients for film and substrate if inelastic effects in the substrate can be ignored. The longitudinal strain component ϵ_3 is generally small, so that errors in the values of the elastic constants for the film do not seriously affect the determination of the total strain. The band-gap shift δE may also be determined directly without the need for the corrections which the transport experiments require.

The use of epitaxial films also appears attractive for producing strains in brittle materials by application of tensile stress to the substrate. In these PbS films, for example, application of uniaxial stress in the [110] direction would shift the [111] band gap by a different amount than the [$\bar{1}$11] band gap. Measurement of both of these gap shifts would therefore allow determination of the two deformation potentials Z_d and Z_u defined by Herring and Vogt.[40]

G. Effective Masses

There are two methods for determining effective mass parameters from the plots presented in Figs. 9 and 11. A mass may be defined in terms of the spacing between two adjacent lines at some fixed field or in terms of the slope of some given line with respect to the magnetic field. Referring to Eq. (5.1) the spacing of the lines is given by $\hbar\omega_{vc}=\hbar eB/m_{vc}c$ while the slope is given by $(l+\frac{1}{2})e/m_{vc}c$ where m_{vc} represents the reduced effective mass $m_vm_c/(m_v+m_c)$. While the masses defined by Eq. (5.1) should all be equal, the experimentally determined masses may not be. Nonparabolic bands, exciton effects and plasma effects will alter the slopes and spacings of the lines in a manner not taken into account in the simple model.

Errors in assigning the correct line position to a given transition will also lead to apparent variations in the reduced effective mass even though the simple model does apply. The latter error arises from the effects of the finite relaxation time and the effects of free carriers on the line shape for the Landau transitions. Both of these effects tend to shift the peak of a given Landau transition to higher energy. These shifts are small, less than $\hbar/\tau$ for the relaxation time shift, and are estimated to be less than 5 meV in the samples measured. The error will tend to cancel for the mass determined from the spacing between lines since they are shifted in the same direction by approximately the same amount. The masses determined from the slopes will tend to reflect this error, particularly for the lowest line which has proportionally the highest error.

In order to minimize the errors associated with assigning a line position, the experimental data were plotted as the ratio of the transmission in magnetic field to the transmission in zero field. The data were taken either at fixed magnetic field as shown in Figs. 7 and 8 or at fixed photon energy as shown in Fig. 10. The line positions for data as in Figs. 7 and 8 were taken at the minimum of the transmission ratio. This corresponds to choosing the line positions as the points-of-tangency of the magnetic field absorption curve with an envelope curve that is proportional to the zero-field absorption curve. The line positions for data as in Fig. 10 were taken as the points-of-tangency of the data curve with its envelope curve. This procedure is necessary since the variation of $\omega_{vc}\tau_{vc}$ across the width of the line significantly warps the line shape. Under suitable approximations, it may be shown that this procedure corresponds to the same condition as applied to the data taken at constant magnetic field.

[41] S. I. Novikova and N. Kh. Abrikosov, Fiz. Tverd. Tela **5**, 1913 (1963) [English transl.: Soviet Phys.—Solid State **5**, 1397 (1964)].

[42] R. M. Buffington and W. M. Latimer, J. Am. Chem. Soc. **48**, 2305 (1926); B. Yates and C. H. Tanter, Proc. Phys. Soc. (London) **80**, 373 (1962).

[43] W. Paul, M. De Meis, and L. X. Finegold, in *Proceedings of the International Conference on the Physics of Semiconductors, Exeter 1962* (The Institute of Physics and the Physical Society, London, 1962), p. 712.

[44] A. A. Chudinov, Fiz. Tverd. Tela **5**, 1458 (1963) [English transl.: Soviet Phys.—Solid State **5**, 1061 (1963)].

The values for the reduced effective mass as determined from the line spacings in Fig. 9 were within 1% of the value $0.0515m_0$. The values determined from the slope of the lines approached this value for the upper lines. The slope of the $l=1$ line gave a value 4% lower for the reduced effective mass. The values for the reduced effective mass from the line spacings in Fig. 11 were all within 3% of the value $0.055m_0$. The values determined from the slope were 8% lower for the $l=1$ line but tended to approach this value for the higher lines. The variations in the value for the reduced effective mass for a given sample are attributed to the effects of the free carriers on the line shape. The difference between the two values for the reduced effective mass for the two different samples is of the proper magnitude and sign to be attributed to the difference in energy gap between the strained and unstrained sample.

The masses determined for other epitaxial crystals with carrier concentrations of the order 10^{18} cm^{-3} tended to fall 2 or 3% lower than the value for the purer crystal quoted above. The masses determined from the slopes also varied over a wider range. This is believed to be due to the increased distortion of the line shape by the higher free-carrier concentration.

The masses determined from the π spectrum for NOL sample No. 108 agreed with the values obtained from the σ spectrum. Small differences between the π and σ masses were observed in the epitaxial crystals with larger carrier concentrations.[37]

The value for the reduced effective mass $m_{vc}=0.055m_0$ for the unstrained crystal is in reasonable agreement with the value $m_{vc}=0.058m_0$ calculated from the values for the electron and hole masses from the free-carrier Faraday rotation measurements. The free-carrier measurements were taken at a somewhat higher temperature with a larger experimental error indicating that the valence and conduction masses at 77°K are probably lower than the values quoted in Sec. III but still within the error limits quoted. For **B**11[100], the cyclotron effective mass is equal to the Faraday effective mass so that the difference is not due to anisotropy.[45]

H. Anisotropy

Energy-band extrema located at points other than Γ in **k** space are not expected to be spherical since the interband matrix elements that determine the effective mass components in different directions are not the same.[46] For ellipsoidal and parabolic bands, the effective mass for cyclotron resonance is given by[2]

$$1/m_i^{\theta}=(1/m_i^{t})[\cos^2\theta+(1/K_i)\sin^2\theta]^{1/2}, \quad (5.5)$$

where θ is the direction between the magnetic field and the major axis of the energy ellipsoid, m_i^t is the transverse effective mass and K_i is the anisotropy ratio or ratio of the longitudinal to transverse effective mass for the ith band. If the transverse effective masses and anisotropy ratios are known for both valence and conduction bands, then it is possible to calculate the reduced effective mass for interband transitions for any given field direction. The converse is not true. It is not possible to infer uniquely the anisotropy of individual bands from a measurement of the anisotropy of the reduced effective mass. However, a spherically symmetric reduced effective mass would tend to imply spherically symmetric individual masses since otherwise, both oblate and prolate ellipsoids with specific antisotropies would be required.

If it is assumed that the valence- and conduction-band ellipsoids are both prolate or both oblate and oriented along the ⟨111⟩ directions, then the number and position of the interband resonance lines will vary with the orientation of the magnetic field. With the magnetic field along the [100] crystal axis a single set of transitions should be observed, since the field axis is symmetric with respect to all of the ⟨111⟩ ellipsoid axes. With the magnetic field along the [110] crystal axis two sets of transitions should be observed, one set with a spacing characteristic of a heavier reduced effective mass and another set characteristic of a lighter reduced effective mass.

The σ spectra were measured on epitaxial PbS samples with the magnetic field oriented along the [100] and along the [110] crystal axes. No resolvable splitting was observed although there was a discernible change in line shapes. The spacing between the lines also remained the same, within experimental error, although the absolute positions were different. The change in absolute position amounted to less than 2 meV and could well be due to the alteration in line shape for the two field orientations. An upper limit on the magnitude of the anisotropy ratio was determined from an estimate of the resolution limit for the experiment. The value $|K|<1.5$ obtained for each band assumes that the anisotropies for the valence and conduction bands are equal. Magnetoresistance experiments on n- and p-type PbS at room temperature,[47] piezoresistance experiments on n-type PbS at nitrogen temperatures[48] and de Haas–van Alphen experiments on n-type PbS at helium temperature[35] all indicate approximately spherical bands.

I. Interband Faraday Rotation

The interband Faraday rotation in n-type PbS exhibits an interesting behavior with variations in free-carrier concentration and the temperature.[20] In the low-carrier concentration range ($N<10^{17}$ cm^{-3}), the rotation is positive at room temperature and remains

[45] M. R. Ellett and K. F. Cuff, Bull. Am. Phys. Soc. **9**, 293 (1964).

[46] G. L. Bir and G. E. Pikus, Fiz. Tverd. Tela **4**, 2243 (1962) [English transl.: Soviet Phys.—Solid State **4**, 1640 (1963)].

[47] R. S. Allgaier, Phys. Rev. **119**, 554 (1960).

[48] Yu. V. Ilisavskii and E. Z. Yakhind, Fiz. Tverd. Tela **4**, 1975 (1962) [English transl.: Soviet Phys.—Solid State **4**, 1447 (1963)].

positive at lower temperatures. In the intermediate range, the rotation is positive at room temperature and changes sign at some lower temperature. In the high-carrier concentration range ($N>10^{18}$ cm^{-3}) the rotation is negative at room temperature and remains negative at lower temperatures. The reversal of the rotation for a sample with a carrier concentration in the intermediate range is shown in Fig. 2. At room temperature the rotation shows the sharp positive rise at short wavelengths that is characteristic of pure and of p-type PbS. At low temperatures, however, the rotation reverses sign and goes sharply negative at short wavelengths.

Such a strong influence on an interband effect by a relatively small number of free carriers is rather unusual but may be explained in terms of the nearly equal valence- and conduction-band parameters of PbS. We shall give a simple physical explanation for the effect here. A more complete treatment is planned for later publication.

The Faraday rotation may be treated as the dispersion effect associated with the absorption of left- and right-circularly polarized (lcp and rcp) radiation. Dispersion relations have been developed[9,11] which relate the rotation to the absorption of lcp and rcp radiation. For example, a single lcp absorption line will lead to a Faraday rotation that has a dispersion tail producing negative rotations at photon energies below the transition energy and positive rotation tail at higher photon energies. For simple bands the lcp and rcp absorption curves should be of approximately equal strength but displaced in energy by an amount and direction that depends on the magnitudes and signs of the effective g factors for the valence and conduction bands. In PbS, the g factors are approximately equal and opposite in sign, so that the lcp and rcp absorptions for a pure crystal are almost superposed. As may be seen in Fig. 6, the rcp absorption line for the lowest Landau transition does lie to slightly lower energy than the lcp line. The rotation to lower photon energies should then be dominated by the positive tail from the rcp line and the tails from the higher lying rcp Landau transitions (assuming the same g factors for the upper Landau levels). This is just the behavior that is observed in pure crystals.

When free carriers are added to the conduction band, the lcp and rcp absorption for a given Landau transition are no longer equal. As discussed in Sec. V, the Fermi distribution of carriers in the conduction band will selectively populate the lower of the two spin states associated with a given Landau level. This weakens one of the two transitions; in PbS the rcp transition is weaker. Consequently, the lcp transitions to those levels in the conduction band that lie within several kT of the Fermi energy will be stronger than the rcp transitions. It is possible then, for the negative rotation dispersion tails associated with the lcp absorption to dominate the positive tails arising from the weak gyromagnetic splitting. Previous attempts[20] to explain this effect involved the introduction of additional bands. However, present knowledge of the band structure indicates that this may not be necessary.

It is desirable to measure the strong-field Faraday rotation at 4.2°K. At this temperature, the free carriers are sharply degenerate and oscillations in the sign of the rotation should be observed with increasing magnetic field as the individual $m=\frac{1}{2}$ and $m=-\frac{1}{2}$ levels are successively pulled through the Fermi level.

VI. BAND STRUCTURE

The results of these experimental studies on PbS at 77°K indicate that the valence- and conduction-band edges are nondegenerate, except for spin, and lie at or very near to the $\langle 111\rangle$ zone boundaries. The anisotropy and nonparabolicity of the bands are both less than the detection limit for the experiments. The effective masses and also the gyromagnetic splitting factors for the valence and conduction bands are approximately equal.

Certain features of the band structure are not unexpected while other features are quite surprising. The location of the extrema at the L points in the Brillouin zone and the lack of higher than twofold spin degeneracy are not unusual. There has been some prior experimental evidence[35] for this location of the conduction band and also evidence that the valence and conduction band extrema nearly coincide in $\mathbf{k}$ space.[24,36] These are also the positions experimentally established for the band extrema in PbTe.[35,49] The lack of higher than twofold degeneracy at the L point is also expected and results from the lifting of the higher degeneracies by the spin-orbit interaction. This is discussed by Pikus and Bir[13] who have developed the variants of the band structure that are permissible according to group theory. It is also discussed by Johnson, Conklin, and Pratt[14] who have specifically calculated the energies and symmetries of the interacting bands at the L point of the Brillouin zone for PbTe including the spin-orbit interaction and other relativistic terms which they find to be important.

The absence of any significant anisotropy, however, is quite unusual. While previous experimental evidence[35,47,48] does indicate almost isotropic bands at 77°K the effective masses derived from theoretical treatments should, in general, be anisotropic and only approach isotropy for particular ordering and energy spacings for the interacting bands at the L point. The main contribution to the curvature of the energy bands at the extrema may be determined by calculation of the $\mathbf{k}\cdot\mathbf{p}$ perturbation between a given band and other interacting bands.[12] For interaction between only the valence and conduction bands at the L point, the $\mathbf{k}\cdot\mathbf{p}$ perturbation calculation does not give isotropic effective masses.[13] This indicates that interaction with additional bands must be taken into account in order to properly explain

[49] K. F. Cuff, M. R. Ellett, and C. D. Kuglin, in *Proceedings of the International Conference on the Physics of Semiconductors, Exeter 1962* (The Institute of Physics and the Physical Society, London, 1962), p. 316.

the apparent isotropy of the energy bands in PbS.[49a] Experiments at 4.2°K would also be of interest since the relative contribution to the effective mass from the valence-conduction band interaction should increase at the smaller band-gap energy and thus alter the anisotropy.

The approximate equality of the valence- and conduction-band effective masses and effective g factors is qualitatively what would be expected from the $\mathbf{k}\cdot\mathbf{p}$ interaction of closely adjacent simple bands. Bir and Pikus[45] have derived a relation between the transverse effective masses for the valence and conduction bands. The effect of one other band, split off by the spin-orbit interaction, is included but the effects of the relativistic terms discussed by Johnson, Conklin, and Pratt[14] are not. Furthermore, interactions with other bands are neglected. They obtain:

$$\frac{m_v^t(1-m_c^t)}{m_c^t(1+m_v^t)}=\begin{cases}1+\lambda & \text{(case a)}\\ 1 & \text{(case b)}\end{cases}, \tag{6.1}$$

where case "a" corresponds to the same choice of symmetry types for the extrema of the valence and conduction bands that are given for PbTe by Johnson, Conklin, and Pratt.[14] The factor λ is defined as $E_g/(E_g+\Delta)$ where E_g is the energy gap and Δ is the spin-orbit splitting of the valence band. The conduction band is simple for case "a." For case "b," the conduction band as well as the valence band arise from the spin-orbit splitting of degenerate bands with opposite parity. The experimental effective masses, determined from the free-carrier Faraday rotation, are both equal within experimental error. Neglecting the possible anisotropy of the bands, the values determined for the masses are not consistent with Eq. (6.1) since they lead to values for this ratio which are less than unity. It is possible to bring this ratio up to one by adjusting the valence and conduction masses within the error limits but keeping the reduced effective mass constant at the value $0.055m_0$. The reduced mass is more accurately known than the individual masses. This comparison would appear to favor case "b" given above, for it would require adjustment of the effective mass values outside of the error limits and abnormally large values for the spin-orbit splitting in order to fit Eq. (6.1) for case "a." However, a positive assignment of the character of the valence and conduction bands cannot be established without a more accurate $\mathbf{k}\cdot\mathbf{p}$ perturbation calculation which includes the interaction with the other valence and conduction bands. Also, it is not obvious that the other $\mathbf{k}$-dependent perturbations which arise from the spin-orbit and other relativistic terms in the Hamiltonian[14] can be neglected as is done in the usual $\mathbf{k}\cdot\mathbf{p}$ calculation. A proper calculation using the five experimentally determined parameters for the effective masses, g factors, and energy gap should clarify the relative ordering of the several interacting bands and give approximate values for some of the energy separations between the bands. Certain of these separations have been determined by Cardona and Greenway[50] from their analysis of transmission and reflectivity measurements extending to 20 eV. The precise identification of these transitions is somewhat hampered, by the multiplicity of choices that arise when transitions at all points in $\mathbf{k}$ space are considered. The additional information given by a $\mathbf{k}\cdot\mathbf{p}$ calculation using band-edge parameters at the point L should prove useful in limiting the ambiguity in the assignments.

VII. CONCLUSIONS

Epitaxial, natural, and synthetic crystals of PbS ranging in carrier concentration from 3×10^{17} to 6×10^{18} cm^{-3} have been investigated at 77°K by a variety of magneto-optical techniques in addition to measurement of the Burstein-Moss shift of the zero-magnetic-field absorption edge.

The free-carrier Faraday rotation experiments on n- and p-type bulk crystals of PbS at temperatures just above 77°K yielded values of $m_c=(0.118\pm0.01)m_0$ for the conduction effective mass and $m_v=(0.115\pm0.01)m_0$ for the valence effective mass.

Structure was observed in the rotation for p-type crystal indicating the proximity in energy of other valence bands. The observation, previously reported, of a reversal in sign of the interband Faraday rotation with increasing carrier concentration and/or decreasing temperature may now be explained as a natural consequence of the near equality of the effective g factors for the valence and conduction bands.

Measurement of the Burstein-Moss shift of the zero-field band edge for a known carrier concentration in the conduction band indicated that the carriers were distributed over four energy bands implying band extrema at the ⟨111⟩ Brillouin zone boundaries. The fits of the theoretical curve to the experimental curve is somewhat less satisfactory for ⟨100⟩ zone boundary extrema although this possibility cannot be definitely excluded by this experiment alone. However, the lack of strain splitting of the interband magneto-optical transitions for ⟨100⟩ oriented crystals appears to rule out this possibility.

The line shapes for the interband magneto-optical

[49a] *Note added in proof.* Pikus and Bir neglect the spin orbit and other relativistic mixing of the L_6^+ or L_6^- states which arise from different single group states. If these interactions are included, then both longitudinal and transverse components of the momentum matrix element are coupled between bands with L_6 symmetry and opposite parity. [See J. O. Dimmock and G. B. Wright, Phys. Rev. **135**, A821 (1964).] Leonard Kleinman and Pay Jun Lin (private communication) and also G. W. Pratt, Jr. and L. G. Ferreira (private communication) have theoretically calculated a large mixing of the levels in PbTe. The same should be true of PbS since its band-gap energy is also small compared to the spin-orbit energy.

[50] M. Cardona and D. L. Greenway, Phys. Rev. **133**, A1635 (1964).

transitions indicate that the valence- and conduction-band extrema both lie at or very near to the same point in **k** space. The position of these lines, extrapolated to zero field, give values for the energy gap of $E_g=(0.279\pm0.002)$ eV for the backed epitaxial crystals, $E_g=(0.309\pm0.005)$ eV for an n-type natural crystal containing 6×10^{18} cm^{-3} free carriers, and $E_g=(0.307\pm0.005)$ eV for a free epitaxial crystal with a low-carrier concentration. The equality, within experimental error, of the latter two values indicates that the energy gap is independent of carrier concentration up to 6×10^{18} cm^{-3}. The difference between these values and the value 0.279 eV given for the epitaxial crystals on backings is due to the strain in these crystals arising from the difference in thermal expansion between the film and the substrate. The effective deformation potential $Z^p=(4.3\pm0.6)$ eV was determined from this gap shift. The reduced effective mass was calculated from the spacing of the interband transition lines. A value of $(0.055\pm0.003)m_0$ was obtained for the natural crystal and $(0.0515\pm0.002)m_0$ for the pure epitaxial crystal on a backing. The anisotropy of the reduced effective mass was <1.5. Values for the effective g factor of 10.0 ± 1.5 for the conduction band and -8.5 ± 1.5 for the valence band were obtained from the observed splitting of the π and σ spectra. The presence of only a single set of evenly spaced Landau transitions indicates that both band edges are nondegenerate, except for spin.

The existence of nondegenerate band extrema at the $\langle111\rangle$ zone boundaries in PbS is not unusual as similar bands have been established experimentally and calculated theoretically for the related semiconductor PbTe. The lack of significant anisotropy, however, is somewhat unusual and indicates the need for a better $\mathbf{k}\cdot\mathbf{p}$ calculation of the band parameters than is currently available. Such a calculation, using the experimentally determined effective masses, effective g factors and energy gap, should also aid in determining the symmetry types and position in energy of other interacting bands at the L point of the Brillouin zone.

ACKNOWLEDGMENTS

The epitaxial crystals, which proved particularly valuable to this study, were grown and their electrical properties were measured by E. G. Bylander, J. D. Jensen, and R. B. Schoolar of the U. S. Naval Ordnance Laboratory. Thanks are due to R. J. Allgaier, J. R. Dixon, and H. R. Riedl, also of the Naval Ordnance Laboratory, for supplying some of the natural and synthetic crystals, for performing Hall measurements and for exchanging unpublished data. Other natural crystals of PbS were obtained from the Natural History Museum of the Smithsonian Institution through the kind cooperation of P. Desautels. A. H. Mister, R. C. Anonsen, W. D. Cline, and J. F. Donnelly provided the magnetic fields and assisted in the experiments.

Particular thanks are due to R. F. Wallis for the many discussions and critical contributions which helped both in the interpretation and the presentation of this work. One of the authors (D.L.M.) wishes to acknowledge discussions with G. W. Pratt and M. Cardona and to thank them for preprints of their work.